The electron density distribution in alpha -tin from powder X-ray data by the maximum-entropy method

1995 J. Phys.: Condens. Matter 7 6961

(http://iopscience.iop.org/0953-8984/7/34/018)

J. Phys.: Condens. Matter 7 (1995) 6961–6966. Printed in the UK

The electron density distribution in α-tin from powder x-ray data by the maximum-entropy method

K Nakahigashi† and K Higashimine‡

† College of Integrated Arts and Sciences, University of Osaka Prefecture, Sakai, Osaka 593, Japan

‡ JAIST-Hokuriku, Nomi-Gun, Ishikawa 923-12, Japan

Received 25 April 1995

Abstract. The electron density distribution map of α-tin has been drawn by the maximum-entropy method (MEM) with 11 independent and two combined structure factors, which were determined by the powder pattern decomposition from x-ray data. The final R and R_w factors were 0.80% and 0.89%, respectivly, though a small amount of β-tin was contained in the specimen. The obtained map indicates that the bonding electrons are clearly seen between the two adjacent tin atoms in the (110) plane with the 0.6 e Å^{-3} level. This value was about twice that of germanium. The structure factor $F(222)e^{-M}$ for the 222 forbidden reflections at 293 K calculated from the MEM density is +0.4350. The results are discussed by comparing with the electron density maps of C (diamond), Si and Ge.

1. Introduction

As is well known, tin exists in two types of stable form. The high-temperature form with a body-centred tetragonal structure, β-Sn (white tin), is stable above 286 K. Below this temperature, α-tin (grey tin) with a diamond structure is stabilized. However, the main experimental work on α-tin hitherto reported was focused on the kinetics of the $\beta \rightarrow \alpha$ phase transformation. For example, Izumi [1] examined the phase transition kinetics by the real-time neutron diffraction studies. Further, Mitchell and Donnellly [2] studied the transformation by transmission electron microscopy and suggested that the transformation was massive in nature. On the other hand, Price and Rowe [3] studied the crystal dynamics of α-tin by means of thermal neutron inelastic scattering and obtained the phonon frequency–wavevector dispersion relation. In contrast with a small amount of experimental work on α-tin, many theoretical studies on the substance have been reported. For example, Svane [4] calculated the Hartree–Fock band structure and cohesive energy by the linear muffin tin orbital method. Brudevoll *et al* [5] calculated the electronic structure within the local density approximation and the resulting band structures were used to obtain effective masses and hydrostatic deformation potentials of α-tin. Although special interest has been devoted to the kinetics of the phase transformation and the electronic band structures, other experimental works, such as an accurate measurement of the crystal structure factors for x-ray diffraction, were lacking.

Sakata and Sato [6] drew the precise electron density distribution map of Si by the maximum-entropy method (MEM) with 30 structure factors which were determined from Pendellösung oscillation by Saka and Kato [7]. The results indicated that the bonding electron was clearly visible in the map, even though no forbidden reflections were included

0953-8984/95/346961+06$19.50

in the analysis. Takata and Sakata [8] evaluated the value of the electron density at the middle point between the neighbouring C atoms of diamond. The present authors and colleagues [9] have also obtained the electron density distribution of Ge and the result indicates that the bonding electron with a level of about 0.3 e $Å^{-3}$ is clearly visible in the map. It is well known that C (diamond), Si, Ge and Sn (α-Sn) in group IV of the periodic table have the same crystal structure and their bonding natures are characterized by covalent bonding. As described above, the bonding electrons of the former three substances were well estimated, and furthermore the respective structure factors, together with their signs, of the forbidden 222 reflection were calculated from the MEM density. However, no experiments on α-tin are available. The reason is due to that it is very hard to obtain a single α-phase and usually the powder sample contains β-phase. In the previous studies of the electron density distribution on AlN [10] and A15-type Cr [11], though the powder samples used were composed of two phases, AlN + Al and A15-type Cr + bcc Cr, the maps obtained by a combination of x-ray powder diffraction data and MEM were very precise.

In the present paper, we give the results of the study of the electron density map and the bonding character of α-tin by the same method as used previously [9–11].

2. Experimental details

The phase transition from β- to α-phase is very difficult when β-tin with high purity is used. Therefore, a dilute alloy $Sn_{0.99}Ge_{0.01}$ was prepared by arc melting appropriate amounts of components Sn and Ge with purity 99.999% . The alloy thus prepared was composed of α- and β-tin. An ingot of pure Sn was joined by partial melting to a portion of the alloy and then was kept in a refrigerator for about 1 d in order to nucleate the α-phase in the ingot. After removing the alloy, the ingot was kept again in a refrigerator to promote a growth of the α-phase. The sample thus obtained was very brittle and was easily smashed into fine pieces by small vibrations. The specimen for x-ray diffraction was obtained by grinding the pieces into powder. The powder thus prepared was composed of α- and β-phase and it was found that the volume fraction of the β-phase was somewhat larger. Therefore the powder was pressed into a pellet and the pellet was further kept in a refrigerator until the volume fraction of the β- (and α-) phase was unchanged. Finally, a fine powder sample of α-tin together with a small amount of β-tin was prepared by grinding in a mortar. Fine particles less than 32 μm in size were selected for powder x-ray diffraction studies.

The powder x-ray diffraction experiment was performed using Cu Kα radiation with a tube voltage of 45 kV and a tube current of 350 mA using an MAC Science M18XHF-SRA-type diffractometer equipped with a curved pyrolytic graphite diffracted beam monochromator. Diffraction intensities were collected by step scanning with a sampling interval of 0.02° in 2θ and an accumulation time of 10 s for every step. In order to remove the statistical counting errors, the sample was rotated around a diffraction vector by a sample spinner. The temperature of the sample was kept at 293 K since the critical temperature of the phase transition from α-phase to β-phase of the present fine particles was near 298 K. In order to confirm that the volume fraction of the respective phases is unchanged during the experiment, the data collection was repeated a few times. In the present experiment, 11 independent and two combined Bragg reflections, i.e. 333(511) and 551(711), of α-tin were observed.

3. Analysis

In order to determine the accurate integrated intensities of respective reflections from the powder x-ray diffraction intensity data, a profile fitting was carried out with the computer program PRO-FIT [12] in which a split Pearson VII function was adopted as a profile function since the peak asymmetry and different decay rates of the low- and high-angle sides of the peak can be modelled explicitly. In the analysis, the intergrated intensity, peak position, full width at half maximum, asymmetric factor and decay rate of each reflection were treated as independent parameters. However, the latter three parameters for the peaks appearing in a small angle range were held constant. Next, the scale factor has to be determined in order to convert the intergrated intensities thus obtained into the structure factors on an absolute scale. This was done by an ordinary least-squares method using the computer program POWLS [13]. In the analysis, only the intergrated intensities of the 11 independent reflections were used. The eight atoms in a unit cell of α-tin are placed at rigid positions. Therefore, the parameters that have to be refined in the analysis are the scale factor and the isotropic temperature factor. The observed independent structure factors are easily calculated from the observed integrated intensities by using the scale factor. The overlapped reflections of 333, 511, 551 and 711 were treated as combined structure factors, which were obtained by taking the square root of the observed integrated intensities after the ordinary corrections and scaling. The structure factors thus determined include the effect on the anomalous dispersion. Then this effect was eliminated from the structure factors by using the values of $\Delta f' = 0.025\,90$ and $\Delta f'' = 5.459\,10$ [14]. The structure factors thus corrected were used as the input data of the following MEM analysis. The procedure of the MEM calculation is the same as in the previous reports [9–11, 15]. In the actual calculation of the MEM, the computer program MEED by Kumazawa *et al* [16] was used. The number of pixels used in the calculation is reduced from $64 \times 64 \times 64$ to 1649 with the aid of the minimum asymmetric unit of the space group $Fd\bar{3}m$.

4. Results and discussion

Typical examples of the profile fits together with differences between the observed and calculated intensities (bottom) are shown in figure 1. In the figure, the crosses and solid curves indicate the observed and calculated intensities, respectively. Figure 1(a) shows the result of the profile fitting of 311 reflections of the α-tin. On the other hand, figure 1(b) shows the decomposition of the overlapped reflections of 331 (α-tin) and 112 (β-tin). Though the intensity of the 112 reflections is somewhat small, the fit is fairly good. The result of the least-squares analysis by POWLS are tabulated in table 1 together with the weighted R_w factor and an estimated standard deviation in parentheses.

Table 1. A summary of the results of the least-squares refinements by POWLS.

Number of data for α-tin used in POWLS analysis	11
Isotropic temperature factor B (Å^2)	0.287(78)
Scale factor S	0.664(11)
Weighted R factor R_w	0.033

An iteration of 300 times gives convergence in the present MEM analysis. The observed and the calculated structure factors from the final MEM density distribution are tabulated in table 2, where the number in parentheses indicates an estimated standard deviation.

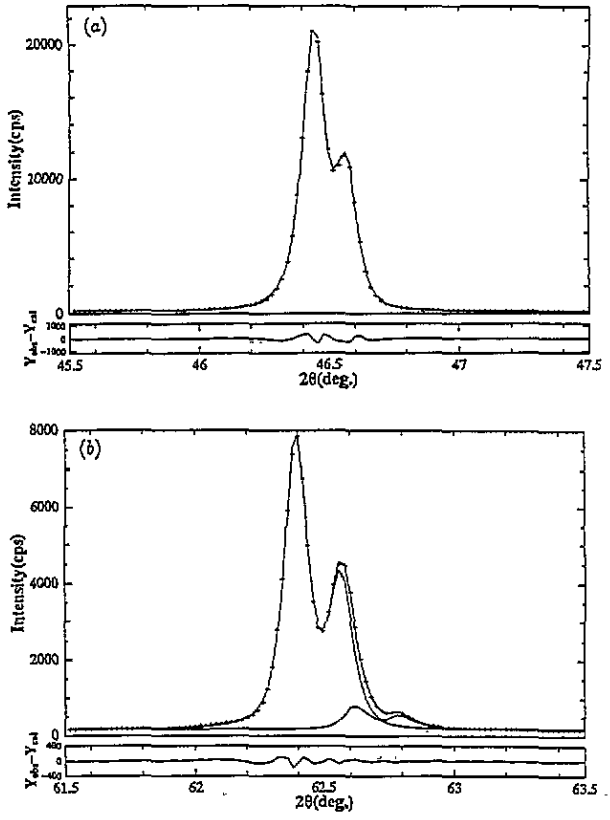

Figure 1. The results of profile fits for (a) 311 (α-tin) and (b) 331 (α-tin) and 112 (β-tin) reflections.

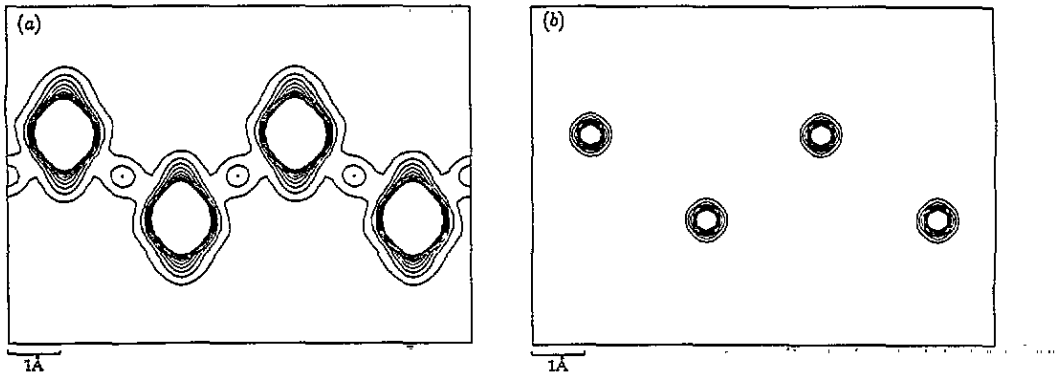

Figure 2. The electron density distribution maps for the (110) plane in α-tin. (a) and (b) are the lower- and higher-electron-density regions. The contour lines (e $Å^{-3}$) are drawn from 0.3 to 3.0 with intervals of 0.3 in (a) and from 40 to 400 with intervals of 40 in (b).

The values of R and R_w factors attained at the final MEM map were 0.80% and 0.87%, respectively. The agreement between observed and calculated structure factors is very good. This indicates that satisfactory electron density distribution is obtained from the observed structure factors. The electron density distribution maps of the lower- and higher-density

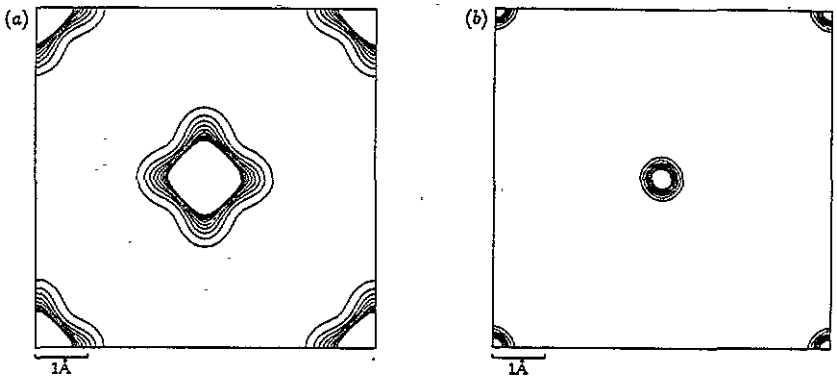

Figure 3. The electron density distribution maps for the (001) plane in α-tin. (a) and (b) are the lower- and higher-electron-density regions. The contour lines (e Å^{-3}) are drawn from 0.3 to 3.0 with intervals of 0.3 in (a) and from 40 to 400 with intervals of 40 in (b).

Table 2. The observed structure factors F_{obs} and G_{obs} and the calculated structure factors F_{calc} from the MEM map.

h k l	F_{obs}	F_{calc}	
1 1 1	−245.8(2.1)	−242.3	
2 2 0	−310.7(2.7)	−308.1	
3 1 1	−210.1(1.8)	−208.3	
4 0 0	−272.5(2.3)	−274.1	
3 3 1	182.4(1.8)	183.0	
4 2 2	243.8(2.1)	241.3	
4 4 0	213.0(1.9)	215.7	
5 3 1	148.0(1.3)	147.8	
6 2 0	199.0(1.7)	198.5	
5 3 3	−128.7(1.2)	−129.4	
4 4 4	−172.5(1.7)	−171.2	
h k l	G_{obs}	G_{calc}	F_{calc}
3 3 3	161.6(1.4)	163.7	161.7
5 1 1			164.4
5 5 1	123.5(1.1)	122.6	−120.4
7 1 1			124.8

regions for the (110) plane of α-tin are shown in figure 2(a) and (b) respectively. The electron density distribution maps of the lower- and higher-density regions for the (001) plane are also shown, for comparison, in figure 3(a) and (b) with the corresponding contour lines to figure 2(a) and (b). No electron densities more than 0.3 e Å^{-3} around the middle points between adjacent atoms can observed in figure 3(a). Therefore, the electron density with the 0.6 e Å^{-3} level observed between the two adjacent tin atoms in figure 2(a) must be due to bonding electrons. The maximum value of the electron density at the atomic sites is 205, 208, 446 and 720 e Å^{-3} for C (diamond) [8], Si [6], Ge [9] and α-Sn, respectively, and it, naturally, increases with increasing atomic number. The value of the electron density at the middle point between the adjacent atoms on the (110) plane was 1.6, 0.7 and 0.3 e Å^{-3} for C (diamond), Si and Ge, respectively. The main part of the chemical bond for these substances is covalent and an s–p hybridized orbital makes the main contribution to the

bond. These values seem to correlate with a bonding strength. In fact the cohesive energy of the three substances decreases with the sequence of C (diamond) → Si → Ge. However, the value of α-tin is twice that of Ge. The bonding strength of α-tin may be weaker than that of Ge. Therefore, we cannot say definitely that the bonding strength correlates with only the value of electron density at the middle point between the adjacent atoms. The maps of the lower-density region for α-tin and Ge are different though those of the higher-density region are very similar. As is clear from figures 2(a) and 3(a), the valence electron density distribution of α-tin, except for the bonding electrons, elongates along ⟨100⟩ directions. On the other hand, the distribution of germanium [9] elongates along ⟨110⟩ directions. These differences in the lower-density region may reflect on their bonding natures.

The structure factor for the 222 forbidden reflection of α-tin at 293 K was calculated by Fourier transformation of the MEM electron density distribution. The value was 0.435 with positive sign. On the other hand, the value previously reported for Si [6] and Ge [9] was +1.527 and −1.056, respectively. Takata and Sakata [8] observed successfully an x-ray diffraction profile of the forbidden 222 reflection from a diamond powder sample with the aid of the synchrotron radiation and imaging plates. They indicated that the observed value of the 222 structure factor was 0.97(1). The finite value of the structure factor for the forbidden reflection is due to non-spherical electron density distributions, such as bonding electrons, together with anharmonic and anisotropic thermal vibrations. However, the main contribution to the structure factor of the forbidden 222 reflections in the diamond structure is due to the bonding electrons.

Therefore we conclude that the asymmetric bonding charge distribution of α-tin is smaller than that of C (diamond), Si and Ge.

5. Concluding remarks

The electron density distribution maps of α-tin are drawn by a combination of powder pattern decomposition data and MEM. The bonding electrons are clearly visible with a density of 0.6 e Å^{-3} at the centre of the neighbouring atoms though we used a powder sample which is composed of the two phases. The observed conventional structure factors are in good agreement with the calculated ones from the MEM density distribution. The value of the forbidden 222 structure factor calculated from the MEM density distribution was +0.435.

References

[1] Izumi M 1986 *Physica* B **136** 36–41
[2] Mitchell D R G and Donnelly S E 1991 *Phil. Mag.* A **63** 747–55
[3] Price D L and Rowe J M 1969 *Solid State Commun.* **7** 1433–8
[4] Svane A 1987 *Phys. Rev.* B **35** 5496–502
[5] Brudevoll T, Citrin D S, Cardona M and Christensen N E 1993 *Phys. Rev.* B **48** 8629–35
[6] Sakata M and Sato M 1990 *Acta Crystallogr.* A **46** 263–70
[7] Saka T and Kato N 1986 *Acta Crystallogr.* A **42** 469–78
[8] Takata M and Sakata M 1993 *PF Activity Rep.* **11** 391
[9] Nakahigashi K, Higashimine K, Ishibashi H and Minimagawa S 1993 *J. Phys. Chem. Solids* **54** 1543–8
[10] Nakahigashi K, Ishibashi H and Minimigawa S 1993 *J. Phys. Chem. Solids* **54** 445–52
[11] Ishibashi H, Arita M, Nishida I, Yanase A and Nakahigashi K 1994 *J. Phys.: Condens. Matter* **6** 8681–90
[12] Toraya H 1986 *J. Appl. Crystallogr.* **19** 440–7
[13] Will G, Parrish W and Huang T C 1983 *J. Appl. Crystallogr.* **16** 611–22
[14] Wilson A J M (ed) 1993 *International Tables for Crystallography* vol C (Dordrecht: Kluwer) p 220
[15] Sakata M, Mori R, Kumazawa S, Takata M and Toraya H 1990 *J. Appl. Crystallogr.* **23** 526–34
[16] Kumazawa S, Kubota Y, Takata M, Sakata M and Ishibashi Y 1993 *J. Appl. Crystallogr.* **26** 453–7